

<https://doi.org/10.1038/s42003-025-08228-z>

# Distinct brain age gradients across the adult lifespan reflect diverse neurobiological hierarchies

Check for updates

Nicholas Riccardi<sup>1</sup> ✉, Alex Teghipco<sup>1</sup>, Sarah Newman-Norlund<sup>1</sup>, Roger Newman-Norlund<sup>2</sup>, Ida Rangus<sup>1,3</sup>, Chris Rorden<sup>2</sup>, Julius Fridriksson<sup>1</sup> & Leonardo Bonilha<sup>4</sup>

‘Brain age’ is a biological clock typically used to describe brain health with one number, but its relationship with established gradients of cortical organization remains unclear. We address this gap by leveraging a data-driven, region-specific brain age approach in 335 neurologically intact adults, using a convolutional neural network (volBrain) to estimate regional brain ages directly from structural MRI without a predefined set of morphometric properties. Six distinct gradients of brain aging are replicated in two independent cohorts. Spatial patterns of accelerated brain aging in older adults quantitatively align with the archetypal sensorimotor-to-association axis of cortical organization. Other brain aging gradients reflect neurobiological hierarchies such as gene expression and externopyramidization. Participant-level correspondences to brain age gradients are associated with cognitive and sensorimotor performance and explained behavioral variance more effectively than global brain age. These results suggest that regional brain age patterns reflect fundamental principles of cortical organization and behavior.

‘Brain age’ is an increasingly recognized biological clock used to measure overall brain health<sup>1,2</sup> (Fig. 1A). A ‘global’ brain age is typically estimated in an individual using machine learning models trained to predict chronological age from MRI, assigning a single estimated age for the entire brain<sup>3</sup>. The difference between predicted and chronological age (brain age gap; BAG) is an estimate of the biological age of a brain, reflecting genetic and lifestyle influences<sup>3</sup>. Higher BAG denotes accelerated brain aging, and has been linked to mortality, dementia, and other neurological or psychiatric conditions<sup>4–6</sup>. However, summarizing brain aging as a single global value risks obscuring spatial gradients that govern cortical organization<sup>7–16</sup> (Fig. 1B).

Recent advances enable region-specific brain age estimates directly from T1-weighted images, without relying on predefined structural properties<sup>17,18</sup>. Convolutional neural networks (CNNs) can learn features directly from 3D images that are predictive of age, offering insights into aging that go beyond traditional singular morphometric measures such as grey matter volume<sup>17,18</sup>. These regional brain age metrics provide the opportunity for a more spatially precise approach than traditional global brain age estimates, allowing for the examination of region-specific variability within and across individuals, including how and why such variability emerges (e.g., inherent properties of the cortex or individual differences in

health or lifestyle). However, the neurobiological and behavioral relevance of these regional estimates remain underspecified, especially in neurologically intact individuals. Little is known about whether patterns of regional brain aging have behavioral correlates, or if they follow neurodevelopmental, phylogenetic, or molecular hierarchies<sup>1</sup>. Addressing these knowledge gaps could bridge brain aging metrics to fundamental principles about the organization of the cortex and associated behaviors<sup>7–16</sup>.

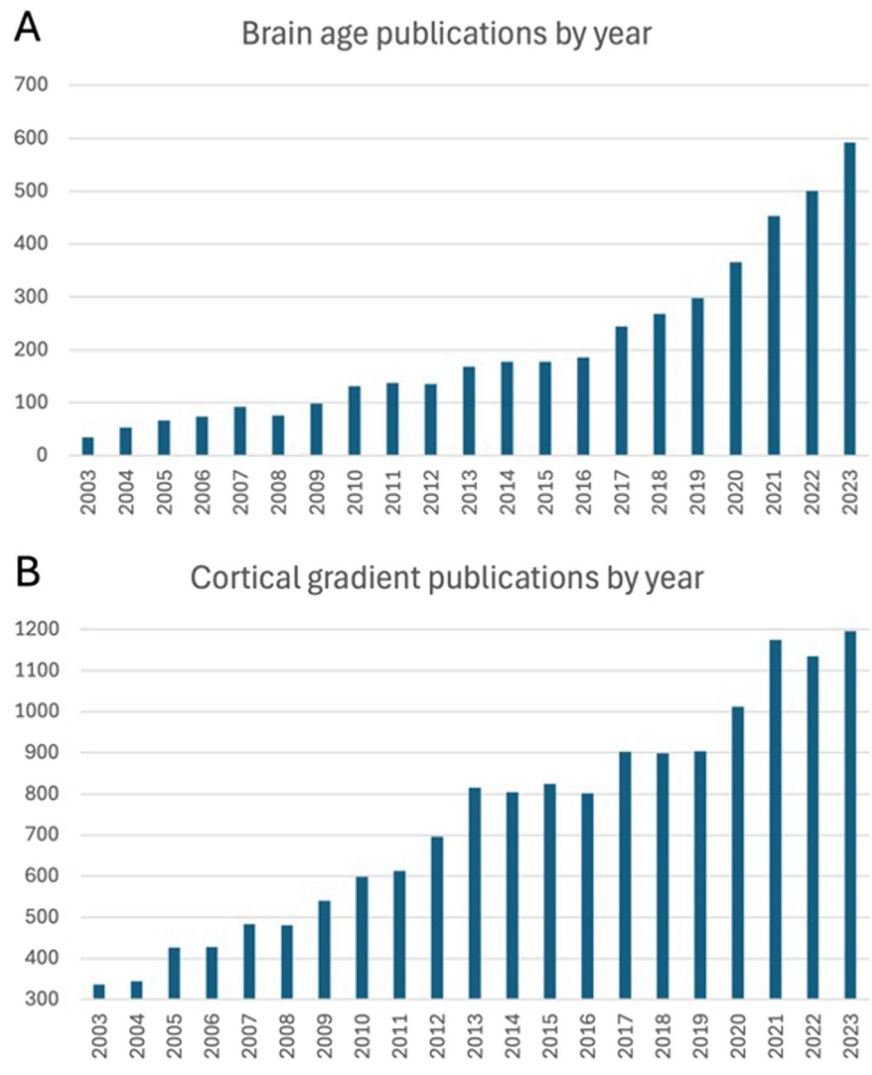
Regional brain aging also provides a novel lens with which to test hypotheses about the cortex. For example, ‘last in, first out’ predicts that late-developing frontal association cortices should age faster or earlier than sensorimotor cortices due to unique metabolic, genetic, or functional properties<sup>19–22</sup>. Further, accelerated aging in functionally specialized regions should relate to domain-specific behavioral decline. While these hypotheses have been supported using traditional morphometrics<sup>19–22</sup>, they are unable to be tested with global brain age and, to our knowledge, have not yet been tested using deep learning-derived regional brain age. As brain age becomes more widely used<sup>1,2</sup>, it is vital to understand how it aligns with known neurobiological constructs.

Here, we examine patterns of regional brain aging in 335 neurologically intact adults (20–86 years) through the lens of the sensorimotor-to-association (S-A) axis of cortical organization<sup>16,23–25</sup>. The S-A axis provides a

<sup>1</sup>Department of Communication Sciences and Disorders, University of South Carolina, Columbia, SC, USA. <sup>2</sup>Department of Psychology, University of South Carolina, Columbia, SC, USA. <sup>3</sup>Center for Stroke Research Berlin, Berlin, Germany. <sup>4</sup>Department of Neurology, School of Medicine Columbia, Columbia, SC, USA.

✉ e-mail: [riccardn@email.sc.edu](mailto:riccardn@email.sc.edu)

**Fig. 1 | Publications related to brain age and cortical gradients.** **A** PubMed query for articles with the phrase “brain age” OR “brain aging” in the title or abstract. **B** PubMed query for articles with the phrases “gradient(s)”, “hierarchy/hierarchical”, or “axis/axes” AND “cortical” or “cortex” in the title or abstract. Both highlight a rapid increase in publications in recent years.



quantitative framework that leverages ten well-validated measures of regional neurobiology, including aerobic glycolysis, cerebral blood flow, cortical thickness, allometric scaling, anatomical and evolutionary hierarchy, gene expression, externopyramidization, and functional neuroimaging meta-analyses<sup>7–16</sup>. Heterogeneous distributions of those cortical properties were mapped using diverse methods such as positron emission tomography (aerobic glycolysis<sup>11</sup>), arterial spin labeling (cerebral blood flow<sup>12</sup>), and primate-human comparative neuroimaging (evolutionary hierarchy<sup>9</sup>). The ‘archetypal S-A axis’ represents a composite map of those properties, where high-ranking areas (association) develop later, are phylogenetically newer, and exhibit distinct functional, structural, and molecular features compared to low-ranking, phylogenetically older sensorimotor regions<sup>16,23–25</sup>. Our primary aim was to determine whether patterns of regional brain aging align with the above hierarchies.

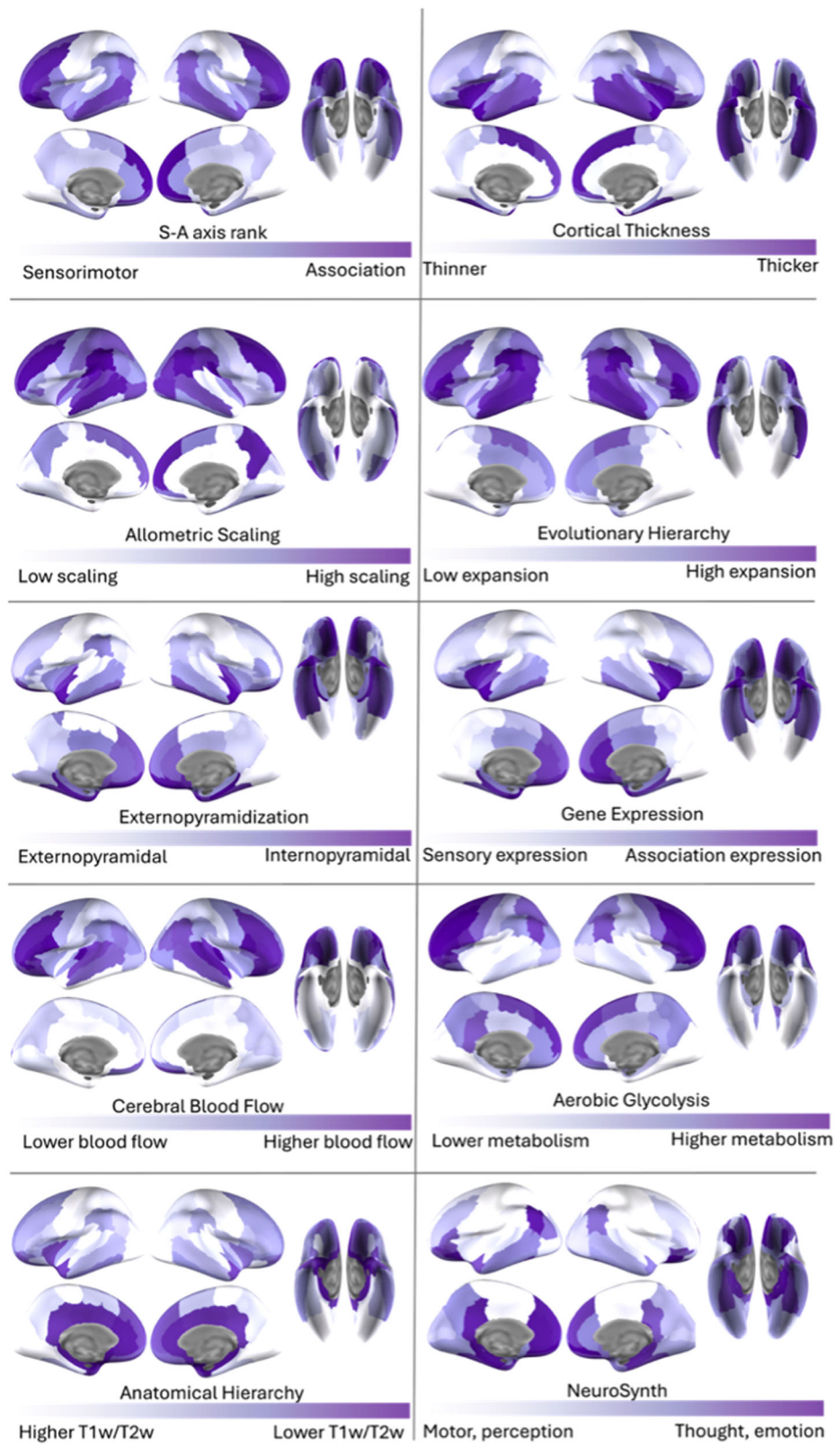
In this context, we found that frontal association cortices show accelerated aging relative to sensorimotor regions in older adults, consistent with the ‘last in, first out’ hypothesis. A data-driven analysis of region-specific brain age gaps (regiBAG) identified six replicable spatial patterns in two independent cohorts. These patterns aligned with specific cortical hierarchies, including the archetypal S-A gradient. Participant-level correspondences to these brain age patterns significantly explained cognitive and sensorimotor performance, even after accounting for demographic factors. Importantly, the regiBAG approach outperformed global brain age (gloBAG) in accounting for behavioral variance. Together, these findings suggest

that spatial patterns of brain aging reflect fundamental principles of cortical organization and may offer a more biologically and behaviorally informative alternative to global brain age.

## Results

We estimated region-specific and global (i.e., ‘whole-brain’) brain ages in 335 neurologically intact adults (20–86 years) using volBrain’s ‘Brain Structure Ages’<sup>18,26</sup>, an automated CNN pipeline trained and validated using thousands of MRIs. It uses features learned directly from T1-weighted images that are predictive of chronological age without relying on predefined morphometric or volumetric properties. This allows for spatially localized age estimates (regional brain ages) which are then, in turn, used as features in a support vector regression framework implemented by volBrain to generate an estimated ‘global’ brain age (see Methods). We calculated region-specific (104 regions) and global BAGs (regiBAG; gloBAG) for each participant by subtracting brain age estimates from chronological age. To quantify neurobiological hierarchies, we used the S-A axis framework<sup>7–16</sup>. Using preexisting vertex-wise data ([https://github.com/PennLINC/S-A\\_ArchetypalAxis](https://github.com/PennLINC/S-A_ArchetypalAxis)<sup>16</sup>), we made 10 cortical maps in volBrain’s parcellation (Fig. 2). These maps consist of regional rankings of the different neuroaxes, wherein higher numerical rankings tend to indicate prototypical association cortices. For all cortical analyses described below, we used parcel-based permutation spin testing ( $p_{\text{spin}}^{27}$ ) to determine correlation significance, which accounts for spatial autocorrelation between two cortical maps.

**Fig. 2 | Sensorimotor-to-association axis and sub-gradients.** Cortical maps for neurobiological gradients in volBrain’s parcellation; vertex-wise values provided by (<sup>16</sup>; [https://github.com/PennLINC/S-A\\_ArchetypalAxis](https://github.com/PennLINC/S-A_ArchetypalAxis)). *S-A axis*<sup>16</sup>: An ‘archetypal’ gradient of sensorimotor-to-association cortices which combined cortical maps from ten fundamental brain features. *Allometric Scaling*<sup>10</sup>: The relative amount of regional expansion to overall brain size in humans. *Externopyramidization*<sup>15</sup>: The ratio of supragranular pyramidal neuron soma size to infragranular pyramidal neuron soma size. *Cerebral Blood Flow*<sup>12</sup>: Blood perfusion as measured by arterial spin labeling. *Anatomical Hierarchy*<sup>7</sup>: The T1-weighted to T2-weighted ratio, which distinguishes sensorimotor-to-association via differences in laminar organization and myelination. *Cortical Thickness*<sup>16</sup>: Quantified from structural MRI provided by the Human Connectome Project S1200. *Evolutionary Hierarchy*<sup>9</sup>: macaque-to-human regional expansion. *Gene Expression*<sup>13</sup>: The first principal component of brain-expressed genes, capturing the greatest fraction of total gene expression variance across cortical areas. *Aerobic Glycolysis*<sup>11</sup>: Quantified from positron emission tomography metrics of glucose use and oxygen consumption. *NeuroSynth PC1*<sup>14</sup>: First principal component of a neuroimaging meta-analysis of 24 terms (e.g., motor, visual perception, emotion, social cognition).



**Spatial patterns of accelerated brain aging in older adults follow the S-A axis**

In 335 participants, we used a two-level analysis to test the ‘last in, first out’ hypothesis<sup>19–22</sup>. For the first level, we assessed relationships between chronological age and regiBAG across the 104 cortical regions using Spearman correlations. This provided a

heterogeneously distributed spatial map of regiBAG x chronological age relationships, identifying areas where older adults exhibited relatively accelerated or decelerated brain aging (Fig. 3B, cortical surface). For the second-level analysis, we compared this spatial map to the maps of 10 neurobiological gradients using  $p_{spin}$  with FDR correction (Fig. 3B, scatterplots).

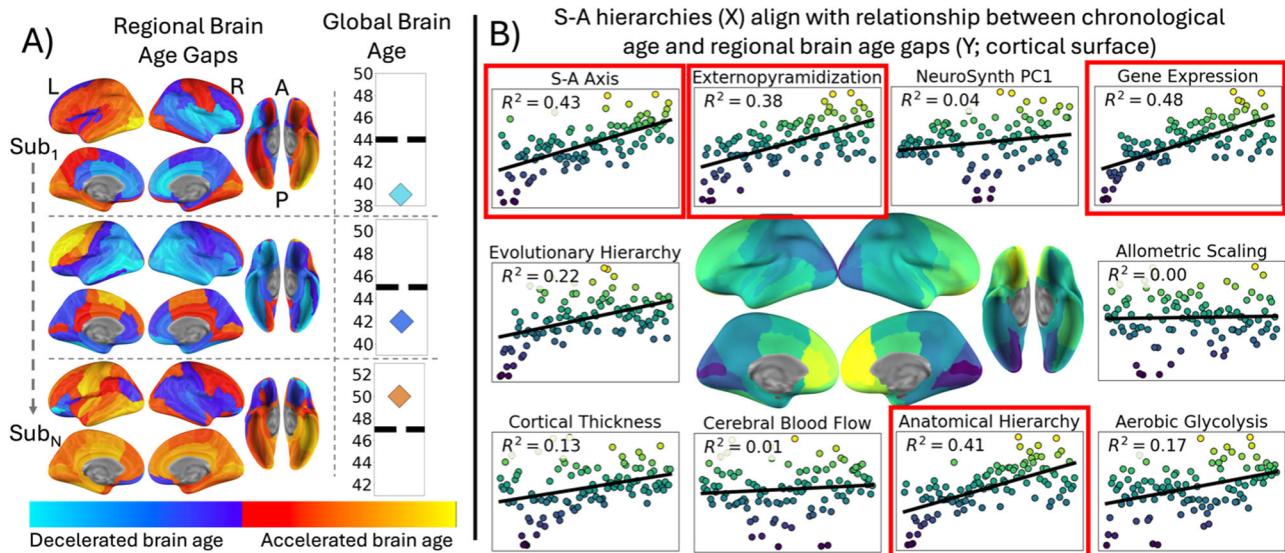


**Fig. 3 | Accelerated regional brain aging in older adults aligns with cortical gradients.** **A** Regional and global brain age estimates for three example participants. Colored diamonds represent global brain age estimates (in years), and the dashed line represents chronological age. **B** Cortical map displaying regional correlations (Spearman's rho) between regional brain age gaps (regiBAGs) and chronological age. Warmer colors (yellow) indicate regions with accelerated aging in older adults relative to cooler colored regions. Scatterplots illustrate second-level analyses

relating this aging pattern to ten established neurobiological gradients of the S-A axis. Each point is a cortical region, with colors matching those on the surface map. X-axes represent each region's rank on an S-A gradient, and Y-axes represent the regional correlations (Spearman's rho) between chronological age and regiBAG from the first-level analysis. Significant correlations ( $p_{\text{spin}}$ , FDR-corrected  $p < 0.05$ ) are indicated by red boxes. Regression lines and corresponding  $R^2$  values are shown for visualization.

The regiBAG x chronological age map was significantly correlated with four gradients: gene expression ( $r_s = 0.67$ ,  $p_{\text{FDR}} = 0.002$ ), the archetypal S-A axis ( $r_s = 0.65$ ,  $p_{\text{FDR}} = 0.002$ ), externopyramidization ( $r_s = 0.58$ ,  $p_{\text{FDR}} = 0.004$ ), and anatomical hierarchy ( $r_s = 0.62$ ,  $p_{\text{FDR}} = 0.003$ ). Late-developing frontal cortices showed accelerated aging relative to sensorimotor cortices in older adults, consistent with the 'last in, first out' hypothesis. Further, these results suggest that three specific cortical properties may underlie region-specific aging vulnerabilities: (1) high transcriptional variability (gene expression), (2) lower neuron density and larger infragranular pyramidal soma size (externopyramidization), and (3) less myelination (anatomical hierarchy).

### Spatial patterns of regional brain age are robust and reflect neurobiological hierarchies

Brain structure varies within and between individuals<sup>16,28</sup>, but whether deep learning-derived regiBAG captures interpretable spatial patterns remains underspecified. To address this, we used exploratory factor analysis (EFA) to identify patterns of regional brain aging in two independent cohorts: our Aging Brain Cohort<sup>29</sup> (ABC;  $n = 167$ ) and a replication group from OpenNeuro (Grady<sup>30-34</sup>;  $n = 158$ ). We chose the Grady data because their participants had a similar age range as the ABC data, were neurologically intact, and because many other publicly available datasets (e.g., UKBioBank, CamCan) had already been used to train volBrain's CNN model.

ABC: EFA revealed six factors of brain aging (KMO = 0.96; Bartlett's  $\chi^2 = 67,143.84$ ,  $p < 0.001$ ), explaining 95% of total variance: Factor 1 – frontal, 31.03%; Factor 2 – dorsal, 29.05%; Factor 3 – ventral, 20.81%; Factor 4 – left frontotemporal, 9.59%; Factor 5 – right temporoparietal, 2.93%; Factor 6 – dorsal frontal, 1.70%.

Grady: EFA yielded six similar gradients (KMO = 0.96; Bartlett's  $\chi^2 = 63,831.37$ ,  $p < 0.001$ ), with 95% variance explained and similar spatial distributions: Factor 1 – frontal, 27.31%; Factor 2 – dorsal, 24.59%; Factor 3 – ventral, 23.26%, Factor 4 – left frontotemporal, 17.52%, Factor 5 – right temporoparietal, 2.39%; Factor 6 – medial, 1.37%.

Pairwise  $p_{\text{spin}}$  between each of the six identified ABC and Grady factors (e.g., F1 vs. F1, F2 vs. F2, etc.) revealed that they were significantly correlated ( $r_s$  range: 0.74–0.95; all two-tailed  $p_{\text{FDR}} < 0.008$ ; SI Table 1; SI Fig. 1). This

suggests that the identified brain age patterns are reproducible in independent datasets, and that they are not likely to be artifacts of study-specific noise or spatial autocorrelation.

Considering the consistency of these findings, we combined the two datasets ( $N = 335$ ) and repeated the EFA, which again identified six factors (Fig. 4A). Areas with higher factor loadings in each pattern are those where accelerated brain aging contributed most strongly to the variance explained. Critically, none of the six factors were significantly correlated with one another (pairwise  $p_{\text{spin}}$   $r_s$  range:  $-0.66$  to  $0.27$ ;  $p_{\text{FDR}} > 0.42$ ; SI Table 2), suggesting that each factor captures a partially distinct brain aging pattern.

We then tested whether these six brain aging patterns align with 10 S-A neuroaxes. Two-tailed  $p_{\text{spin}}$  tests were performed for each factor against all 10 neurobiological gradients, with FDR correction applied per factor. Regional loading scores from four of the six factors were significantly correlated with neurobiological hierarchies (Fig. 4B). Factor 1 (frontal) was related to gene expression ( $r_s = 0.75$ ,  $p_{\text{FDR}} < 0.001$ ), the archetypal S-A axis ( $r_s = 0.48$ ,  $p_{\text{FDR}} = 0.05$ ), externopyramidization ( $r_s = 0.69$ ,  $p_{\text{FDR}} < 0.001$ ), and anatomical hierarchy ( $r_s = 0.70$ ,  $p_{\text{FDR}} < .001$ ). Factor 2 (dorsal) was negatively correlated with externopyramidization ( $r_s = -0.60$ ,  $p_{\text{FDR}} = 0.03$ ) and NeuroSynthPC1 ( $r_s = -0.61$ ,  $p_{\text{FDR}} = 0.03$ ). Factor 3 (ventral) was negatively correlated with the archetypal S-A axis ( $r_s = -0.58$ ,  $p_{\text{FDR}} = 0.02$ ) and aerobic glycolysis ( $r_s = -0.71$ ,  $p_{\text{FDR}} = .002$ ). Factor 4 (left frontotemporal) was correlated with the archetypal S-A axis ( $r_s = 0.24$ ,  $p_{\text{FDR}} = 0.02$ ) and evolutionary hierarchy ( $r_s = 0.26$ ,  $p_{\text{FDR}} = 0.02$ ). Factors 5 and 6 were not significantly correlated with any of the S-A neuroaxes. Taken together, these findings suggest that established neuroaxes are latent constructs that underlie emergent gradients of regional brain aging.

### Spatial patterns of brain aging are related to cognitive, sensory, and motor performance

Here, we examined whether the identified brain age gradients have neuroanatomically sensible relationships with behavior, and we compared their explanatory power to an alternative approach using global brain age gaps. Using the six factors derived from the combined ABC and Grady EFA ( $N = 335$ ), we extracted participant-level factor scores reflecting how strongly each individual's brain aging pattern matched each factor (Fig. 5).

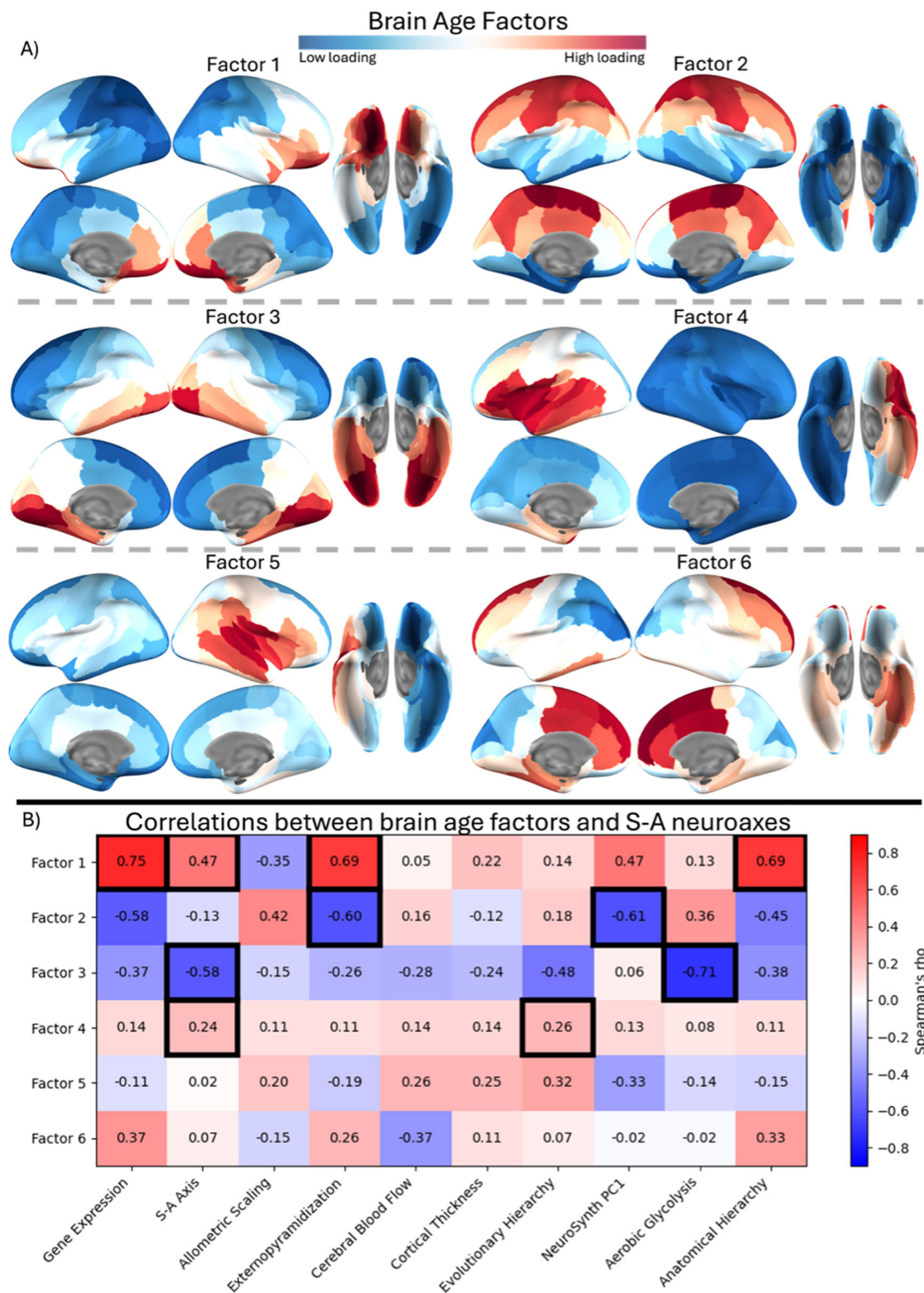


**Fig. 4 | Gradients of regional brain aging.** **A** The six identified regiBAG factors (brain age gradients) from the combined ABC and Grady EFA, with regional loading scores displayed on cortical surfaces. Red indicates higher loading in the identified factor. **B** The heatmap shows Spearman's rho for pairwise comparisons between the factor maps and S-A neuroaxes. Black boxes indicate significant correlations,

determined via  $p_{\text{spin}}$  tests with FDR correction ( $p_{\text{FDR}} < 0.05$ ). Note that, with  $p_{\text{spin}}$  testing, medium-to-strong correlations between two cortical maps can be insignificant if their spatial pattern closely matches what could arise by chance due to spatial autocorrelation.

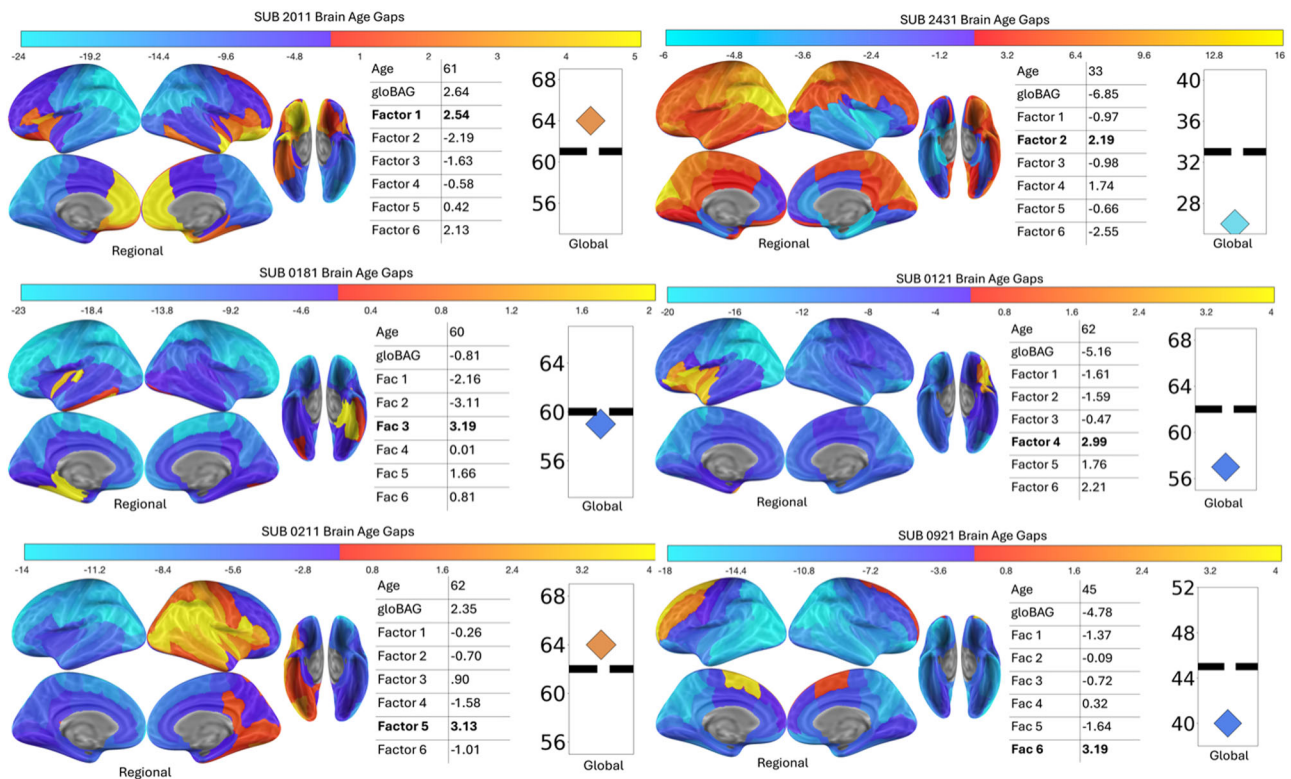


**Fig. 5 | Individualized patterns of brain aging revealed by factor scores.** Exemplar participants for each identified factor, with the highest factor score for each participant indicated in bold. Regional and global brain age gap color scales are centered around a brain age gap of 0. Global brain age estimates are shown with colored diamonds, and chronological age is shown with a dotted black line. Participant-level

factor scores, chronological age, and gloBAG are provided in the corresponding tables. regiBAG factor analysis allowed for patterns of accelerated regional brain aging to be captured and related to cognitive, sensory, and motor performance in neurologically intact adults.

We then used these factor scores as predictors in stepwise linear regression models, along with age, sex, and education, to explain behavioral variance. Critically, participant-level factor scores were orthogonal ( $r_s$  range:  $-0.05$  to  $0.06$ ;  $p^*_{s_{uncorrected}} > .32$ ; SI Table 3). Because behavioral data were unavailable for the Grady cohort, regression analyses were limited to the ABC group ( $N = 167$ ). For global brain age, separate stepwise linear regression models were used, with global brain age gap, age, sex, and education as the independent variables. Cognitive status was assessed with the Montreal Cognitive Assessment (MoCA<sup>35</sup>). Multimodal sensory abilities were assessed with the National Institutes of Health (NIH) Visual Acuity Test<sup>36</sup> (vision) and a pure tone threshold test (hearing). Gross motor skills were assessed with the NIH Standing Balance Test (balance) and 4-meter walking gait speed (locomotion)<sup>37</sup>.

MoCA score variance was significantly explained by a model including age, education, and scores from Factors 5 and 6 ( $F(4,162) = 19.0, p < 0.001, \text{adj. } R^2 = 0.3$ ). Factors 5 and 6 (right temporoparietal and medial) significantly improved model fit (Factor 5  $\Delta R^2 = 0.04, p = 0.005$ ; Factor 6  $\Delta R^2 = 0.02, p = 0.04$ ). Visual acuity variance was significantly explained by age, education, and Factor 3 ( $F(3, 163) = 26.2, p < 0.001, \text{adj. } R^2 = 0.31$ ). Scores from Factor 3 (ventral visual stream) significantly improved model fit ( $\Delta R^2 = 0.02, p = 0.02$ ). Hearing variance was significantly explained by age, education, and Factor 5 ( $F(3, 163) = 78.7, p < 0.001, \text{adj. } R^2 = 0.58$ ), with Factor 5 (right temporoparietal) significantly improving model fit ( $\Delta R^2 = 0.01, p = 0.04$ ). With the combined ABC/Grady EFA approach, brain age patterns did not significantly contribute to model fit for balance or locomotion. However, using the factor scores from the ABC-only EFA, variance in balance was significantly explained by age and Factor 2 scores ( $F(2, 155) = 10.15, p < 0.001, \text{adj. } R^2 = 0.1$ ), and variance in locomotion (gait speed) was significantly explained by age, sex, and Factor 6 scores ( $F(3, 163) = 5.35, p = 0.002, \text{adj. } R^2 = 0.07$ ). In the alternative models using global

brain age gaps instead of factor scores, global brain age gaps did not improve model fit for any behavioral measure beyond age, sex, and education.

## Discussion

Neurobiological gradients govern the spatial organization of the cortex<sup>16,23–25</sup>. We investigated how these gradients are reflected in regional brain age patterns derived from deep learning<sup>17</sup>. We provided five findings: (1) Frontal association cortices exhibited accelerated brain aging relative to sensorimotor cortices in older adults; (2) Six brain aging gradients replicated across independent datasets; (3) Four of these gradients corresponded to established neuroaxes; (4) Participant-level alignment with specific brain aging patterns related to individual differences in cognitive and sensorimotor performance; (5) The regional brain age approach explained behavioral variance better than global brain age gaps. These findings highlight the promise of regional brain age as biomarkers that bridge established cortical principles and behavior.

The heterogeneous pattern of brain aging across the lifespan was organized anteriorly-to-posteriorly (Fig. 3B). In older adults, frontal association cortices displayed accelerated aging relative to sensorimotor cortices, supporting the ‘last in, first out’ hypothesis<sup>19–22</sup>. This map of brain aging across the lifespan aligned with the archetypal S-A axis, gene expression, externopyramidization, and anatomical hierarchy. Thus, three cortical properties appear particularly relevant to regional aging susceptibility: (1) high transcriptional variability (gene expression), (2) lower neuron density and larger infragranular pyramidal soma size (externopyramidization), and (3) lower myelination (anatomical hierarchy). These properties may mechanistically underpin the vulnerability of association cortices to accelerated aging. For example, regions with high transcriptional variability have greater expression of genes related to neurodegeneration<sup>13</sup>, while areas with inherently less myelination may be

more vulnerable to deleterious effects of metabolic stress, inflammation, and oxidative damage<sup>38–40</sup>.

Factor analysis revealed six reproducible brain aging gradients, four of which significantly aligned with S-A neuroaxes. Factor 1, primarily medial frontal, resembled the map of accelerated aging in older adults identified in Fig. 3B and mirrored the archetypal S-A axis, gene expression, extero-pyramidization, and anatomical hierarchy. These neuroaxes capture areas with protracted development and plasticity, which, when combined with inherently high transcriptional variability, less myelination, and lower neuron density, may amplify susceptibility to both modifiable and non-modifiable neurodegenerative risk factors<sup>41–43</sup>. These convergent molecular and cellular features provide a plausible mechanistic basis for why Factor 1 explained the largest share of variance in the brain aging patterns.

Factor 2 revealed a dorsal pattern (motor and superior parietal cortices), negatively correlating with the pyramidal map and NeuroSynthPC1. These areas are continuously engaged during everyday sensorimotor demands<sup>14</sup>, have high neuron density<sup>14</sup>, and are heavily myelinated<sup>7</sup>, making them generally robust against age-related deterioration<sup>19,22,45</sup>. However, prior work in older adults has found that cardiovascular health and physical fitness are associated with preserved integrity of the dorsal ‘action’ pathway<sup>46,47</sup>. Thus, this brain age pattern is a promising candidate as a dimension of brain health that, while having inherently ‘robust’ cortical properties, may be sensitive to modifiable factors such as physical activity.

Factor 3, resembling the ventral visual stream, negatively correlated with the archetypal S-A axis and aerobic glycolysis. These regions have low metabolic demands, and, like the above-mentioned dorsal stream, are typically robust against age-related atrophy<sup>19,22,45</sup>. However, ventral stream deterioration is associated with visual impairments and cognitive decline, which often coincide<sup>48–50</sup>. Given our own results linking this brain age gradient to visual acuity, Factor 3 emerges as a promising candidate for exploring mechanistic links between vision, brain health, and cognition.

Factor 4, centered around left frontotemporal cortices, correlated with the archetypal S-A axis and evolutionary expansion. These regions are phylogenetically newer, as determined via primate-human comparative neuroimaging<sup>9</sup>. We suggest that this brain aging pattern represents portions of the canonical language network, given its left-lateralization<sup>51</sup>, alignment with evolutionary expansion (language is a recent evolutionary adaptation<sup>52</sup>), and overlap with regions important for language<sup>53–55</sup> (e.g., Broca’s area). While this language-related interpretation awaits further testing, identification of this factor suggests that phylogenetically newer, left-lateralized cortices represent a distinct dimension of brain aging.

Factors 5 and 6 loaded heavily on right temporoparietal and bilateral medial areas, respectively. They did not significantly align with the S-A neuroaxes and may instead correspond with alternative hierarchies not tested here, such as those capturing neurogenesis or archicortical patterning<sup>56–60</sup>. They may also reflect individual, health-related differences (e.g., Factor 5’s relationship to hearing, see below) rather than general neurobiological hierarchies. Also of note, Factors 4 and 5 were lateralized. Replication of these gradients in independent datasets suggests that they are not artifacts of noise. We contend that they reflect genuine lateralized patterns, which would be consistent with known functional asymmetries in the brain (e.g., language: typically left<sup>51</sup>; visuospatial attention: typically right<sup>61</sup>). The degree of lateralization can vary among individuals<sup>62,63</sup>, which may explain why certain participants exhibit more pronounced lateralized brain aging patterns than others. Previous research using alternative approaches has also found evidence for lateralized cortical gradients<sup>56,64,65</sup>.

Finally, participant-level correspondences to specific brain age gradients explained behavioral variance beyond chronological age, sex, and education. Participants that more closely matched Factor 5 (right temporoparietal) had worse hearing and cognitive status, demonstrating a promising shared neural substrate for the link between hearing loss and cognitive decline<sup>66–69</sup>. Brain aging in the bilateral ventral stream was associated with worse visual acuity, validating regional brain aging with the neuroanatomical ‘ground truth’ that the ventral stream is vital for visual

processing and shape recognition<sup>70–72</sup>. Factors 2 and 6 (dorsal and medial) significantly explained variance in walking gait and standing balance scores, again highlighting sensible brain-behavior relationships, this time in dorsal ‘action’ stream areas<sup>73–75</sup>. Importantly, identifying these brain-behavior relationships required the regional brain age approach. Global brain age gaps did not explain variance beyond demographic variables. This suggests that future studies examining brain-behavior associations using brain age could benefit from a regional approach similar to the one employed here.

There are several limitations and possible extensions of this work. This study was cross-sectional and cannot determine causality between brain age and behavior. Longitudinal designs could explore how brain age changes within individuals over time, and how this relates to behavior. We focused our analyses on 10 gradients within the S-A axis framework. Other established gradients exist<sup>56–60</sup>, which could provide additional information about cortical properties that underlie brain age patterns. Although subcortical structures are also given brain age estimates by volBrain, we restricted our analyses to cortical regions to directly compare our findings to established cortical S-A gradients; future studies should explicitly explore how subcortical brain age relates to health and behavior, as these regions would also be expected to have meaningful variations in structure within and across individuals. Regional brain age approaches in patient populations may provide novel insights about brain health and clinical outcomes. While our brain-behavior effect sizes were modest, it is important to recognize that our neurologically intact cohort had relatively restricted behavioral and neuroanatomical variability. Finally, future work should clarify how specific modifiable health factors or individual differences relate to regional brain aging.

In conclusion, we identified robust and reproducible spatial patterns of regional brain aging and linked them to established neuroaxes. Cortical properties of high gene expression, low neuron density, and large infragranular pyramidal soma size, and less myelination underlie a dominant pattern of brain aging, centered around frontal association cortices. This provides mechanistic insights into regional vulnerabilities to aging that future studies could leverage to better understand or prevent brain health decline. Additionally, the relationships between brain aging patterns and behavior validate the functional significance and interpretability of these data-driven gradients. With the growing recognition of brain age as a meaningful biological clock, this work provides a vital foundation for research aiming to identify modifiable factors, mechanisms, and interventions that can promote healthier brain aging trajectories.

## Methods

### Participants

167 participants aged 20–80 (mean = 48.8 yo; 125 female; Table 1) were recruited as part of the University of South Carolina’s ongoing Aging Brain Cohort project (ABC<sup>29</sup>) and had available neuroimaging and behavioral measurements. ABC focuses on neurologically intact, community-dwelling adults. It has the following exclusion criteria: history of stroke, diagnosis of neurodegenerative disease, serious acute or chronic conditions that would limit their ability to participate, any severe current illnesses (e.g., cancer), psychiatric diagnosis (e.g., schizophrenia), or anyone with a BMI of > 42 kg/m<sup>2</sup>. Participants were native English speakers. All study procedures were approved by the Institutional Review Board of the University of South Carolina. Written informed consent was obtained from each participant. All ethical regulations relevant to human research participants were followed. The replication data (Grady<sup>30–33</sup>) consisted of 158 participants aged 20–86 (mean = 49.46 yo; 99 female). They were free from major psychiatric or neurological conditions, cognitively normal (MMSE > 26), and fluent English speakers.

### Tasks, measurements, and procedures

**Cognitive.** Participants completed the Montreal Cognitive Assessment (MoCA<sup>35</sup>). Trained research associates administered the MoCA after completing the official MoCA Training and Certification course. Note that, although all participants were independent and community-

**Table 1 | Demographic, behavioral, and brain age variables for ABC data**

Demographics	Mean or %	SD or N
Sex, female	74.8%	125
Age, years	48.8	19.7
Education, level (1 = elementary school; 7 = graduate degree)	5.1	0.9
Cognitive		
MoCA score	27.4	2.4
MoCA score $\leq$ 25	22.7%	38
Sensory		
Pure tone threshold	12.2	13.5
NIH visual acuity	108.3	13.8
Motor		
NIH Standing Balance	105.1	9.8
NIH 4-meter gait speed	3.6	0.7
Brain age		
Global brain age gap	-1.4	4.7
Global brain age > chronological age	35.9%	60

dwelling, with no diagnosis of cognitive impairment or neurological disorders, participants displayed a relatively wide range of scores (19 to 30) with 22.7% of participants scoring in the at-risk range for MCI ( $\leq 25$ <sup>35</sup>; Table 1).

**Sensory.** Two sensory tasks were administered by trained research associates to measure hearing and vision. Hearing: a pure-tone audiometric threshold test (PTT) administered in a soundproof booth using the Amplivox 170 audiometer/headphone set. Participants indicated when they heard a tone, and the audiometer recorded the minimum level (threshold) in decibels at which the tone was reliably detected (detected at least 2/3 times presented). The test covered the following frequencies for both ears: 250 Hz, 500 Hz, 1000 Hz, 2000 Hz, 3000 Hz, 4000 Hz, 6000 Hz, and 8000 Hz. A single PTT score was calculated for each participant in accordance with the criteria established by the World Health Organization<sup>76</sup>: for each frequency, we selected the lower (better) threshold between their left and right ears, and then averaged across all frequencies. A higher PTT score indicates worse hearing.

Vision: the National Institutes of Health (NIH) Visual Acuity Test was administered<sup>36</sup>. It assesses corrected distance vision by having participants sit 3 meters away from an 11-inch iPad and verbally identify single letters that appear on the screen. The letters get progressively smaller, and lower scores indicate worse vision.

**Motor.** To measure locomotion and balance, we used the NIH 4-Meter Walk Gait Speed Test and NIH Standing Balance Test<sup>37</sup>. In the 4-meter walk, participants are timed as they are instructed to walk 4 meters at a normal speed on a flat surface, specifically at the speed at which they would walk down the street. Participants are given a practice trial, and then two real trials, and their speed in the two trials is averaged to create a final score. For balance, participants are asked to perform a series of poses on a foam pad. It involves the participant assuming and maintaining five poses for 50 seconds each. The sequence of poses is: eyes open on a solid surface, eyes closed on a solid surface, eyes open on a foam surface, eyes closed on a foam surface, and eyes open in tandem stance on a solid surface. Postural sway is recorded for each pose using an accelerometer worn at waist level.

**MRI acquisition.** ABC: T1-weighted images were collected for each participant using a Siemens Prisma Fit 3 T scanner with a 20-channel

head/neck coil and the following parameters: 3D MP-RAGE sequence, voxel size = 1 × 1 × 1 mm; field of view = 256 × 256 × 192 mm; preparation repetition time = 2530 ms; inversion time = 925 ms; flip angle = 9°; echo time = 4.11 ms; GRAPPA x2 acceleration (80 reference lines).

Grady: T1-weighted images were collected for each participant using a Siemens Trio 3 T scanner and the following parameters: 3D MP-RAGE sequence, voxel size = 1 × 1 × 1 mm; field of view = 256 mm; acquisition matrix = 192 × 256 × 160; repetition time = 2000 ms, echo time = 2.63 ms.

**Brain age estimation.** Global and regional brain age estimates were calculated using volBrain's BrainStructureAges<sup>18,26</sup>, an automated, publicly available pipeline which takes un-preprocessed T1-weighted images as input. BrainStructureAges estimates brain age through a multi-step deep learning process. First, brain structures are parcellated into 133 ROIs with AssemblyNet, a validated deep learning ensemble of 3D U-Net models trained to replicate high quality manual segmentations of microanatomical brain regions made by expert radiologists and neuroanatomists according to the BrainCOLOR protocol<sup>77,78</sup>. The model integrates multiple overlapping subvolumes, refining segmentation accuracy by leveraging the strengths of different U-Net models. A separate U-Net model ensemble was trained to predict chronological age at the voxel level from raw T1-weighted image signal. These models employ convolutional and deconvolutional layers to progressively learn spatial patterns and features in the MR image that are most predictive of chronological age, without relying on predefined morphometric features like cortical thickness or volume. This results in a single, 'global' estimated brain age for each individual based on the entire brain, as well as a heterogeneous map of region-specific age estimates for each individual. The heterogeneous maps allow for more spatially precise investigations of how variations in regional brain structure (which arise due to participant-level genetic or health factors, or due to general cortical properties) relate to behavior or to established neurobiological gradients.

volBrain was trained and tested on thousands of MR images from various datasets, with chronological ages ranging 5 to 85. As part of the model training to estimate voxelwise brain age, each preprocessed T1-weighted MRI (registered to MNI space as part of volBrain's preprocessing pipeline, with dimensions 181×217×181 voxels at 1 mm<sup>3</sup> resolution) was first downsampled by a factor of two, resulting in a lower-resolution 91 × 109 × 91 voxel image. Next, overlapping sub-volumes of size 32×48×32 voxels were extracted across the downsampled image. Specifically, 125 sub-volumes were evenly spaced along the three spatial dimensions, ensuring full coverage. Each sub-volume was then used to train a separate U-Net model to predict voxel-wise chronological age. This resulted in 125 independently trained U-Net models, each contributing to a reconstructed 3D age map of 91 × 109 × 91 voxels. For regions where voxels appeared in multiple overlapping sub-volumes, predictions were averaged across models to reduce variability. This 3D age map was upsampled using trilinear interpolation to match the original MRI resolution and is used to derive regional and global brain age estimates.

During training, each voxel within the intracranial cavity (ICC) was assigned the participant's chronological age as its ground truth value, while voxels outside the ICC were set to zero. The models were optimized using stochastic gradient descent (SGD) with the mean absolute error (MAE) as the loss function. Training was performed in mini-batches of 8 images, with an early stopping criterion of 20 epochs if no improvement in validation loss was observed. The first U-Net was trained from scratch, while the remaining models were initialized using transfer learning from neighboring U-Nets to enhance efficiency. Training data was split into 80% training and 20% validation sets, and each time a new U-Net was trained, the training/validation split was redefined to maximize the use of available data. To mitigate overfitting, random spatial shifts were applied, as well as mixup augmentation, which combines patches from different subjects to improve generalization. To validate the chronological age prediction in an independent testing set, they computed the regional brain ages of the U-Nets' training subjects. This data was then used to train a support vector regression-based

**Table 2 | Stepwise linear regression results**

DV: MoCA	Model 1		Model 2		Model 3		Model 4	
	$\beta$	$p$	$\beta$	$p$	$\beta$	$p$	$\beta$	$p$
Age	-0.483	<0.001***	-0.463	<0.001***	-0.486	<0.001***	-0.502	<0.001***
Sex	0.050	0.463	0.065	0.337	0.060	0.366	0.051	0.435
Education	0.156	0.022*	0.121	0.077	0.138	0.040*	<b>0.138</b>	<b>0.040*</b>
Factor 1	-0.038	0.577	-0.042	0.538	-0.047	0.479	-0.032	0.626
Factor 2	-0.087	0.203	-0.092	0.171	-0.075	0.257	-0.064	0.329
Factor 3	-0.037	0.602	-0.011	0.873	-0.017	0.806	-0.014	0.833
Factor 4	-0.036	0.603	-0.031	0.640	-0.035	0.595	-0.033	0.613
Factor 5	-0.184	0.007**	<b>-0.184</b>	<b>0.007**</b>	<b>-0.209</b>	<b>0.002**</b>	<b>-0.180</b>	<b>0.008**</b>
Factor 6	0.161	0.018*	0.189	0.005**	<b>0.189</b>	<b>0.005**</b>	<b>0.201</b>	<b>0.003*</b>
Adj. R <sup>2</sup> ( $p$ )	0.229 (<0.001***)		0.258 (<0.001***)		0.289 (0.001***)		0.303 (0.001***)	
$\Delta R^2$ ( $p$ )			0.033 (0.007**)		0.035 (0.005**)		0.018 (0.040*)	
DV: Visual Acuity	Model 1		Model 2		Model 3			
	$\beta$	$p$	$\beta$	$p$	$\beta$	$p$	$\beta$	$p$
Age	-0.522	<0.001***	-0.535	<0.001***	-0.577	<0.001***		
Sex	-0.032	0.636	-0.039	0.552	-0.054	0.403		
Education	0.170	0.010*	<b>0.170</b>	<b>0.010*</b>	<b>0.163</b>	<b>0.013*</b>		
Factor 1	-0.029	0.636	-0.011	0.872	-0.016	0.808		
Factor 2	0.025	0.705	0.037	0.575	0.029	0.654		
Factor 3	-0.170	0.013*	-0.162	0.017*	<b>-0.162</b>	<b>0.017*</b>		
Factor 4	-0.086	0.194	-0.083	0.205	-0.063	0.332		
Factor 5	-0.052	0.439	-0.015	0.827	0.006	0.927		
Factor 6	-0.031	0.641	-0.013	0.848	-0.006	0.925		
Adj. R <sup>2</sup> ( $p$ )	0.268 (<0.001***)		0.293 (<0.001***)		0.313 (<0.001***)			
$\Delta R^2$ ( $p$ )			0.029 (0.010*)		0.024 (0.017*)			
DV: Pure Tone Threshold	Model 1		Model 2		Model 3			
	$\beta$	$p$	$\beta$	$p$	$\beta$	$p$	$\beta$	$p$
Age	<b>0.736</b>	<0.001***	<b>0.752</b>	<0.001***	<b>0.732</b>	<0.001***		
Sex	-0.032	0.546	-0.023	0.646	-0.033	0.518		
Education	-0.198	<0.001***	<b>-0.198</b>	<0.001***	<b>-0.178</b>	<0.001***		
Factor 1	-0.020	0.711	-0.041	0.420	-0.037	0.466		
Factor 2	0.026	0.629	0.012	0.808	0.017	0.740		
Factor 3	-0.026	0.641	-0.036	0.496	-0.051	0.337		
Factor 4	0.051	0.337	0.047	0.359	0.045	0.374		
Factor 5	0.145	0.006**	0.106	0.041*	<b>0.106</b>	<b>0.041*</b>		
Factor 6	-0.020	0.712	-0.042	0.414	-0.054	0.289		
Adj. R <sup>2</sup> ( $p$ )	0.539 (<0.001***)		0.576 (<0.001***)		0.584 (<0.001***)			
$\Delta R^2$ ( $p$ )			0.039 (<0.001***)		0.011 (0.041*)			
DV: NIH Standing Balance <sup>+</sup>	Model 1		Model 2					
	$\beta$	$p$	$\beta$	$p$	$\beta$	$p$	$\beta$	$p$
Age	-0.303	<0.001***	-0.329	<0.001***				
Sex	0.024	0.754	0.013	0.866				
Education	0.069	0.369	0.056	0.463				
Factor 1	-0.027	0.722	-0.026	0.732				
Factor 2	-0.158	0.041	<b>-0.158</b>	<b>0.041*</b>				
Factor 3	0.021	0.787	0.013	0.864				
Factor 4	0.044	0.568	0.046	0.542				
Factor 5	-0.025	0.751	-0.022	0.776				
Factor 6	-0.024	0.754	-0.023	0.762				
Adj. R <sup>2</sup> ( $p$ )	0.086 (<0.001***)		0.104 (<0.001***)					
$\Delta R^2$ ( $p$ )			0.024 (0.041*)					

DV: 4-meter gait speed <sup>†</sup>	Model 1		Model 2		Model 3	
	$\beta$	$p$	$\beta$	$p$	$\beta$	$p$
Age	<b>0.201</b>	<b>0.009**</b>	<b>0.212</b>	<b>0.006**</b>	<b>0.229</b>	<b>0.003**</b>
Sex	0.158	0.039*	<b>0.158</b>	<b>0.039*</b>	<b>0.166</b>	<b>0.028*</b>
Education	-0.066	0.387	-0.073	0.334	-0.092	0.226
Factor 1	-0.055	0.474	-0.034	0.663	-0.035	0.643
Factor 2	-0.094	0.225	-0.082	0.289	-0.081	0.290
Factor 3	-0.116	0.138	-0.107	0.166	-0.098	0.200
Factor 4	-0.077	0.316	-0.063	0.406	-0.065	0.385
Factor 5	-0.006	0.935	-0.014	0.851	-0.023	0.758
Factor 6	-0.148	0.053	-0.157	0.038	<b>-0.157</b>	<b>0.038*</b>
Adj. R <sup>2</sup> ( $p$ )	0.035 (.009**)		0.054 (0.004**)		.073 (0.002**)	
$\Delta R^2$ ( $p$ )			0.025 (0.039*)		0.024 (0.038*)	

Models explain variance in cognitive, sensory, and motor tasks using age, sex, education, and participant-level factor scores derived from the combined ABC/Grady EFA. Bold indicates a variable that was added to the significant model at each step. \*\*\* indicates  $p < 0.001$ , \*\* indicates  $p < 0.01$ , \* indicates  $p < 0.05$ . † indicates that, for the motor tasks, we used ABC-only EFA participant-level factor scores. Factor scores did not significantly improve model fit for these two tasks when using the combined ABC/Grady EFA scores. Equivalent models using gloBAG instead of participant-level factor scores did not explain behavioral variance beyond age, sex, and education.

model with 10-fold cross-validation, resulting in 10 separate SVR models. Each test sample was evaluated with all 10 models, and their age estimations were averaged to ensure model generalization. Two out-of-domain datasets were then used to assess model accuracy. These SVR models are used to generate global (e.g., ‘whole-brain’) brain age estimates.

### Regional quantification of the sensorimotor-to-association axis and subcomponents

To quantify the S-A axis and its respective gradient feature maps, thus giving each region in volBrain’s parcellation an average score reflecting its location along the S-A neuroaxes, we used the fsaverage5 vertex-wise metrics provided by (<sup>16</sup>; [https://github.com/PennLINC/S-A\\_ArchetypepalAxis](https://github.com/PennLINC/S-A_ArchetypepalAxis)) and the following steps. First, AssemblyNet is used to segment the MNI152 1 mm space template by directly submitting this map to the volBrain protocol. To achieve more uniform coverage of cortical regions for improving projection onto surface space (i.e., around sulci), each voxel within the cerebrospinal fluid ROI in the segmentation is reclassified by assigning it the label of the nearest cortical voxel based on Euclidean distance. Each ROI within the segmentation is then binarized and independently projected onto the fsaverage surface using a high-quality nonlinear RT-ANTs transformation<sup>79</sup>. A winner-take-all approach is then used to assign ROIs to vertices lying on the boundaries between regions using brainSurfer<sup>80</sup>.

The surface-space segmentation or ‘atlas’ is then downsampled to the fsaverage5 template using FreeSurfer to match the template for the vertex-wise metrics provided by ref. 16. Then, using custom MATLAB scripts, we calculated the vertex-wise average for each ROI for the S-A axis and its subcomponents. Note that we did not include the functional hierarchy measure here due to its strong correlations with gene expression, NeuroSynth PCI, cerebral blood flow, aerobic glycolysis, and cortical thickness<sup>16</sup>, indicating that it is adequately captured by other gradients. The averaged values were then ranked such that lower values for each gradient indicate sensorimotor cortices and higher values indicate association cortices, as was done in ref. 16. Thus, each cortical volBrain ROI ( $N = 104$ ) was bestowed a single rank value for each of the S-A measures (Fig. 2).

### Statistical Analyses

**Parcel-based permutation spin testing.** For all cortical analyses comparing two spatial maps (e.g., Factor 1 vs. S-A axis ranks), we used permutation spin testing ( $p_{\text{spin}}^{27}$ ) via the netneurotools package (<https://github.com/netneurolab/netneurotools>) to account for spatial autocorrelation. Permutation spins randomize spatial correspondences between cortical maps while preserving their intrinsic spatial structure. Cortical surface data for each hemisphere were mapped to a spherical coordinate system using FreeSurfer’s standard left and right hemisphere

spherical surfaces, which aligned cortices to a common spherical mesh while preserving geodesic distances. Non-cortical ROIs were excluded.

For each hemisphere, parcel centroids were computed as the mean spherical coordinates of all vertices within each parcel. To ensure geometric validity for spin rotations, centroids were projected onto the unit sphere by normalizing their Euclidean coordinates. Spins were generated independently per hemisphere by randomly rotating spherical coordinates and subsequently assigning rotated coordinates back to original parcels using the Hungarian algorithm. Using 5000 permutations, values from one map were rotated within each hemisphere and then concatenated to form a null whole-cortex dataset, while the other map’s values remained fixed. The Spearman correlation between maps was then recalculated for each permutation to construct a null distribution. A two-tailed p-value was then computed by comparing the proportion of null correlations to the observed correlation magnitude, with a continuity correction applied to account for finite permutations.

### Spatial patterns of accelerated brain aging in older adults follow the S-A axis

First, for each of the 104 cortical regions, we used nonparametric Spearman’s correlations to extract the strength and direction of the relationship between chronological age and regional brain age gaps. This first-level analysis resulted in a heterogeneous distribution of correlation coefficients across the cortex, representing the relationship between brain age gap and chronological age for each region. Higher values, displayed as brighter yellow in Fig. 3B, indicate regions with relatively higher regional brain age estimates in older participants. Next, the resulting map was compared to maps of 10 neurobiological gradients using  $p_{\text{spin}}$  with FDR correction.

### Spatial patterns of regional brain age reflect neurobiological hierarchies

In SPSS (IBM Corp. Released 2023. IBM SPSS Statistics for Macintosh, Version 29.0.1.0 Armonk, NY: IBM Corp), exploratory factor analysis was conducted using principal axis factoring with the regiBAG correlation matrix. We chose exploratory factor analysis (EFA) with varimax rotation to identify cortical brain age gradients because it explicitly models latent constructs (in our case, hypothesized to be neurobiological gradients), enhances interpretability by ensuring regions load onto distinct factors, and aligns with our goal of capturing distinct, theoretically meaningful dimensions of brain age variation. Factors were kept based on eigenvalues greater than 1, with a maximum of 25 iterations for convergence. Varimax rotation with Kaiser normalization was applied to the extracted factors to enhance interpretability<sup>81</sup>. This rotation method was chosen to minimize the number of brain regions that have high

loadings on each factor, thereby removing multicollinearity for the purpose of using regional and participant-level factor scores for linear regression in subsequent analyses. The regiBAG rotated factor matrix loading scores were extracted for each region for each factor. Two-tailed  $p_{\text{spin}}$  tests were then performed for each factor against all 10 neurobiological gradients, with FDR correction applied per factor.

### Spatial patterns of brain aging are related to cognitive, sensory, and motor performance

Based on the six factors identified above, participant-level factor scores were computed using the regression method in SPSS. These factor scores were subsequently used in five stepwise linear regression models to investigate the relationship between patterns of brain aging and performance on cognitive (MoCA), sensory (visual acuity and PTT), and motor tasks (standing balance and 4-meter gait speed). Each model included nine independent variables: the six factor scores, age, sex, and education, and variables were entered into the model at a significance level of 0.05 and removed at 0.10. Full model results can be seen in Table 2. We compared these models to identical models that used gloBAG instead of the factor scores.

### Statistics and reproducibility

All statistical analyses were conducted as detailed in the Statistical Analyses section. Sample sizes were based on the full set of eligible participants meeting inclusion criteria and were sufficient to ensure statistical power ( $N = 335$ ). Final sample sizes are reported for each analysis. No data points were excluded unless otherwise specified. Statistical tests were selected based on data type and distributional assumptions; all tests were two-sided unless stated otherwise. Multiple comparisons were corrected using false discovery rate (FDR) procedures where applicable. All imaging and behavioral analyses were conducted using pre-specified pipelines applied uniformly across participants. Findings were replicated in two independent cohorts using matched preprocessing and analysis procedures.

### Reporting summary

Further information on research design is available in the Nature Portfolio Reporting Summary linked to this article.

### Data availability

A subset ( $N = 158$ ) of the neuroimaging data used here can be found on OpenNeuro (<https://openneuro.org/datasets/ds005270/versions/1.0.0>; <https://doi.org/10.18112/openneuro.ds005270.v1.0.0>). The S-A axes data can be found at [https://github.com/PennLINC/S-A\\_ArchetypeAxis](https://github.com/PennLINC/S-A_ArchetypeAxis). The regional maps of S-A axes ranks, in volBrain's parcellation, can be found here: <https://doi.org/10.17605/OSF.IO/X8QP9>. The Aging Brain Cohort is an internally funded project with ongoing data collection. Data requests can be made here: <https://abc.sc.edu/abc-repository-data-requests/>.

### Code availability

Brain ages from structural MRI (raw T1s) can be fully and automatically replicated here (<https://volbrain.net/services/BrainStructureAges>), including full preprocessing, segmentation, and brain age estimation.  $p_{\text{spin}}$  was performed with Netneurotools' `gen_spinsamples` ([https://github.com/netneurolab/markello\\_spatialnulls/blob/master/scripts/empirical/generate\\_spin\\_resamples.py](https://github.com/netneurolab/markello_spatialnulls/blob/master/scripts/empirical/generate_spin_resamples.py)). Code for generating parcel maps from vertex-wise S-A axis data, as well as generating parcel maps from regional brain age factor loadings and spin testing, can be found here<sup>82</sup>: <https://doi.org/10.17605/OSF.IO/X8QP9>. These volumetric parcel maps can be automatically projected into the appropriate surface space via brainSurfer's GUI<sup>80</sup> (<https://github.com/alexteghipco/brainSurfer>; <https://doi.org/10.5281/zenodo.7271544>).

Received: 1 November 2024; Accepted: 14 May 2025;

Published online: 25 May 2025

## References

- Gaser, C., Kalc, P. & Cole, J. H. A perspective on brain-age estimation and its clinical promise. *Nat. Comput. Sci.* **4**, 744–751 (2024).
- Baecker, L., Garcia-Dias, R., Vieira, S., Scarpazza, C. & Mechelli, A. Machine learning for brain age prediction: Introduction to methods and clinical applications. *EBioMedicine* **72**, 103600 (2021).
- Cole, J. H. Multimodality neuroimaging brain-age in UK biobank: relationship to biomedical, lifestyle, and cognitive factors. *Neurobiol. Aging* **92**, 34–42 (2020).
- Cole, J. H., Marioni, R. E., Harris, S. E. & Deary, I. J. Brain age and other bodily 'ages': implications for neuropsychiatry. *Mol. Psychiatry* **24**, 266–281 (2019).
- Busby, N. et al. Lower socioeconomic status is associated with premature brain aging. *Neurobiol. Aging* **130**, 135–140 (2023).
- Busby, N. et al. White matter hyperintensity load is associated with premature brain aging. *Aging*. <https://doi.org/10.18632/aging.204397>. (2022).
- Glasser, M. F. & Van Essen, D. C. Mapping human cortical areas in vivo based on myelin content as revealed by T1- and T2-weighted MRI. *J. Neurosci.* **31**, 11597–11616 (2011).
- Margulies, D. S. et al. Situating the default-mode network along a principal gradient of macroscale cortical organization. *Proc. Natl Acad. Sci. USA* **113**, 12574–12579 (2016).
- Hill, J. et al. Similar patterns of cortical expansion during human development and evolution. *Proc. Natl Acad. Sci. USA* **107**, 13135–13140 (2010).
- Reardon, P. K. et al. Normative brain size variation and brain shape diversity in humans. *Science* **360**, 1222–1227 (2018).
- Vaishnavi, S. N. et al. Regional aerobic glycolysis in the human brain. *Proc. Natl Acad. Sci. USA* **107**, 17757–17762 (2010).
- Satterthwaite, T. D. et al. Impact of puberty on the evolution of cerebral perfusion during adolescence. *Proc. Natl Acad. Sci. USA* **111**, 8643–8648 (2014).
- Burt, J. B. et al. Hierarchy of transcriptomic specialization across human cortex captured by structural neuroimaging topography. *Nat. Neurosci.* **21**, 1251–1259 (2018).
- Yarkoni, T., Poldrack, R. A., Nichols, T. E., Van Essen, D. C. & Wager, T. D. Large-scale automated synthesis of human functional neuroimaging data. *Nat. Methods* **8**, 665–670 (2011).
- Paquola, C. et al. A multi-scale cortical wiring space links cellular architecture and functional dynamics in the human brain. *PLoS Biol.* **18**, e3000979 (2020).
- Sydnor, V. J. et al. Neurodevelopment of the association cortices: Patterns, mechanisms, and implications for psychopathology. *Neuron* **109**, 2820–2846 (2021).
- Cole, J. H. et al. Predicting brain age with deep learning from raw imaging data results in a reliable and heritable biomarker. *Neuroimage* **163**, 115–124 (2017).
- Nguyen, H. D., Clement, M., Mansencal, B. & Coupe, P. Brain structure ages—A new biomarker for multi-disease classification. *Hum. Brain Mapp.* **45**, e26558 (2024).
- Raz, N. & Rodrigue, K. M. Differential aging of the brain: patterns, cognitive correlates and modifiers. *Neurosci. Biobehav. Rev.* **30**, 730–748 (2006).
- Douaud, G. et al. A common brain network links development, aging, and vulnerability to disease. *Proc. Natl Acad. Sci. USA* **111**, 17648–17653 (2014).
- Filippi, M. et al. Age-related vulnerability of the human brain connectome. *Mol. Psychiatry* **28**, 5350–5358 (2023).
- Raz, N. et al. Regional brain changes in aging healthy adults: general trends, individual differences and modifiers. *Cereb. Cortex* **15**, 1676–1689 (2005).
- Larsen, B., Sydnor, V. J., Keller, A. S., Yeo, B. T. T. & Satterthwaite, T. D. A critical period plasticity framework for the sensorimotor-

- association axis of cortical neurodevelopment. *Trends Neurosci.* **46**, 847–862 (2023).
24. Sydnor, V. J. et al. Intrinsic activity development unfolds along a sensorimotor-association cortical axis in youth. *Nat. Neurosci.* **26**, 638–649 (2023).
  25. Keller, A. S. et al. Hierarchical functional system development supports executive function. *Trends Cogn. Sci.* **27**, 160–174 (2023).
  26. Nguyen, H. D., Clement, M., Mansencal, B. & Coupe, P. Towards better interpretable and generalizable AD detection using collective artificial intelligence. *Comput. Med. Imaging Graph.* **104**, 102171 (2023).
  27. Markello, R. D. & Misisic, B. Comparing spatial null models for brain maps. *Neuroimage* **236**, 118052 (2021).
  28. Lemaitre, H. et al. Normal age-related brain morphometric changes: nonuniformity across cortical thickness, surface area and gray matter volume?. *Neurobiol. Aging* **33**, 617 e611–617 e619 (2012).
  29. Newman-Norlund, R. D. et al. The Aging Brain Cohort (ABC) repository: The University of South Carolina’s multimodal lifespan database for studying the relationship between the brain, cognition, genetics and behavior in healthy aging. *Neuroimage: Rep.* **1**. <https://doi.org/10.1016/j.yinrp.2021.100008>. (2021).
  30. Rieck, J. R., Baracchini, G., Nichol, D., Abdi, H. & Grady, C. L. Reconfiguration and dedifferentiation of functional networks during cognitive control across the adult lifespan. *Neurobiol. Aging* **106**, 80–94 (2021).
  31. Rieck, J. R., Baracchini, G. & Grady, C. L. Contributions of brain function and structure to three different domains of cognitive control in normal aging. *J. Cogn. Neurosci.* **33**, 1811–1832 (2021).
  32. Rieck, J. R., DeSouza, B., Baracchini, G. & Grady, C. L. Reduced modulation of BOLD variability as a function of cognitive load in healthy aging. *Neurobiol. Aging* **112**, 215–230 (2022).
  33. Grady, C. L., Rieck, J. R., Baracchini, G. & DeSouza, B. Relation of resting brain signal variability to cognitive and socioemotional measures in an adult lifespan sample. *Soc. Cogn. Affect Neurosci.* **18**, nsad044 (2023).
  34. Rieck, J. R. et al. BOLD variability during cognitive control for an adult lifespan sample. *OpenNeuro* [Dataset] <https://doi.org/10.18112/openneuro.ds005270.v1.0.0> (2024).
  35. Nasreddine, Z. S. et al. The Montreal Cognitive Assessment, MoCA: a brief screening tool for mild cognitive impairment. *J. Am. Geriatr. Soc.* **53**, 695–699 (2005).
  36. Gershon, R. C. et al. NIH toolbox for assessment of neurological and behavioral function. *Neurology* **80**, S2–S6 (2013).
  37. Reuben, D. B. et al. Motor assessment using the NIH Toolbox. *Neurology* **80**, S65–S75 (2013).
  38. Maas, D. A., Valles, A. & Martens, G. J. M. Oxidative stress, prefrontal cortex hypomyelination and cognitive symptoms in schizophrenia. *Transl. Psychiatry* **7**, e1171 (2017).
  39. Tsutsui, S. & Stys, P. K. Metabolic injury to axons and myelin. *Exp. Neurol.* **246**, 26–34 (2013).
  40. Nave, K. A. & Ehrenreich, H. Myelination and oligodendrocyte functions in psychiatric diseases. *JAMA Psychiatry* **71**, 582–584 (2014).
  41. Hou, Y. et al. Ageing as a risk factor for neurodegenerative disease. *Nat. Rev. Neurol.* **15**, 565–581 (2019).
  42. Habes, M. et al. Advanced brain aging: relationship with epidemiologic and genetic risk factors, and overlap with Alzheimer disease atrophy patterns. *Transl. Psychiatry* **6**, e775 (2016).
  43. Rabin, J. S. et al. Association of beta-Amyloid and Vascular Risk on Longitudinal Patterns of Brain Atrophy. *Neurology* **99**, e270–e280 (2022).
  44. Collins, C. E., Airey, D. C., Young, N. A., Leitch, D. B. & Kaas, J. H. Neuron densities vary across and within cortical areas in primates. *Proc. Natl Acad. Sci. USA* **107**, 15927–15932 (2010).
  45. Toga, A. W., Thompson, P. M. & Sowell, E. R. Mapping brain maturation. *Trends Neurosci.* **29**, 148–159 (2006).
  46. Rowley, C. D. et al. Exercise and microstructural changes in the motor cortex of older adults. *Eur. J. Neurosci.* **51**, 1711–1722 (2020).
  47. Northey, J. M. et al. Objectively measured physical activity is associated with dorsolateral prefrontal cortex volume in older adults. *Neuroimage* **221**, 117150 (2020).
  48. Zheng, D. D. et al. Longitudinal associations between visual impairment and cognitive functioning: The Salisbury Eye Evaluation Study. *JAMA Ophthalmol.* **136**, 989–995 (2018).
  49. Chen, S. P., Bhattacharya, J. & Pershing, S. Association of vision loss with cognition in older adults. *JAMA Ophthalmol.* **135**, 963–970 (2017).
  50. Han, G. et al. Decreased visual acuity is related to thinner cortex in cognitively normal adults: cross-sectional, single-center cohort study. *Alzheimers Res. Ther.* **14**, 99 (2022).
  51. Frost, J. A. et al. Language processing is strongly left lateralized in both sexes. Evidence from functional MRI. *Brain* **122**, 199–208 (1999).
  52. Berwick, R. C. & Chomsky, N. *Why Only Us: Language and evolution*. (MIT Press, 2016).
  53. Desai, R. H. & Riccardi, N. In *The Routledge Handbook of Cognitive Linguistics* 615–642 (2021).
  54. Hickok, G. & Poeppel, D. The cortical organization of speech processing. *Nat. Rev. Neurosci.* **8**, 393–402 (2007).
  55. Riccardi, N. & Desai, R. H. In *The Routledge Handbook of Semiosis and the Brain* 174–189 (Routledge, 2022).
  56. Valk, S. L. et al. Shaping brain structure: Genetic and phylogenetic axes of macroscale organization of cortical thickness. *Sci. Adv.* **6**, eabb3417 (2020).
  57. O’Leary, D. D., Chou, S. J. & Sahara, S. Area patterning of the mammalian cortex. *Neuron* **56**, 252–269 (2007).
  58. Chen, C. H. et al. Genetic influences on cortical regionalization in the human brain. *Neuron* **72**, 537–544 (2011).
  59. Charvet, C. J. & Finlay, B. L. Evo-devo and the primate isocortex: the central organizing role of intrinsic gradients of neurogenesis. *Brain Behav. Evol.* **84**, 81–92 (2014).
  60. Huntenburg, J. M., Yeow, L. Y., Mandino, F. & Grandjean, J. Gradients of functional connectivity in the mouse cortex reflect neocortical evolution. *Neuroimage* **225**, 117528 (2021).
  61. Siman-Tov, T. et al. Bihemispheric leftward bias in a visuospatial attention-related network. *J. Neurosci.* **27**, 11271–11278 (2007).
  62. James, J. S. et al. Analyzing functional, structural, and anatomical correlation of hemispheric language lateralization in healthy subjects using functional MRI, diffusion tensor imaging, and voxel-based morphometry. *Neurol. India* **63**, 49–57 (2015).
  63. Greve, D. N. et al. A surface-based analysis of language lateralization and cortical asymmetry. *J. Cogn. Neurosci.* **25**, 1477–1492 (2013).
  64. Labache, L., Ge, T., Yeo, B. T. T. & Holmes, A. J. Language network lateralization is reflected throughout the macroscale functional organization of cortex. *Nat. Commun.* **14**, 3405 (2023).
  65. Xu, X. et al. Spatiotemporal Atlas of the fetal brain depicts cortical developmental gradient. *J. Neurosci.* **42**, 9435–9449 (2022).
  66. Nemat, S., Arjmandi, M., Busby, N., Bonilha, L. & Fridriksson, J. The impact of age-related hearing loss on cognitive decline: The mediating role of brain age gap. *Neuroscience* **551**, 185–195 (2024).
  67. Wang, H. F. et al. Hearing impairment is associated with cognitive decline, brain atrophy and tau pathology. *EBioMedicine* **86**, 104336 (2022).
  68. Panza, F., Solfrizzi, V. & Logroscino, G. Age-related hearing impairment—a risk factor and frailty marker for dementia and AD. *Nat. Rev. Neurol.* **11**, 166–175 (2015).
  69. Griffiths, T. D. et al. How can hearing loss cause dementia?. *Neuron* **108**, 401–412 (2020).

70. Konen, C. S. & Kastner, S. Two hierarchically organized neural systems for object information in human visual cortex. *Nat. Neurosci.* **11**, 224–231 (2008).
71. Kravitz, D. J., Saleem, K. S., Baker, C. I. & Mishkin, M. A new neural framework for visuospatial processing. *Nat. Rev. Neurosci.* **12**, 217–230 (2011).
72. James, T. W., Culham, J., Humphrey, G. K., Milner, A. D. & Goodale, M. A. Ventral occipital lesions impair object recognition but not object-directed grasping: an fMRI study. *Brain* **126**, 2463–2475 (2003).
73. Mihara, M., Miyai, I., Hatakenaka, M., Kubota, K. & Sakoda, S. Role of the prefrontal cortex in human balance control. *Neuroimage* **43**, 329–336 (2008).
74. Bolton, D. A. The role of the cerebral cortex in postural responses to externally induced perturbations. *Neurosci. Biobehav. Rev.* **57**, 142–155 (2015).
75. Taubert, M., Mehnert, J., Pleger, B. & Villringer, A. Rapid and specific gray matter changes in M1 induced by balance training. *Neuroimage* **133**, 399–407 (2016).
76. Humes, L. E. The World Health Organization’s hearing-impairment grading system: an evaluation for unaided communication in age-related hearing loss. *Int. J. Audiol.* **58**, 12–20 (2019).
77. Coupe, P. et al. AssemblyNet: A large ensemble of CNNs for 3D whole brain MRI segmentation. *Neuroimage* **219**, 117026 (2020).
78. de Senneville, B. D., Manjón, J. V. & Coupé, P. RegQCNET: Deep quality control for image-to-template brain MRI affine registration. *Phys. Med. Biol.* **65**, 225022 (2020).
79. Wu, J. et al. Accurate nonlinear mapping between MNI volumetric and FreeSurfer surface coordinate systems. *Hum. Brain Mapp.* **39**, 3793–3808 (2018).
80. brainSurfer v. 2.0.2. <https://doi.org/10.5281/zenodo.7271544>, (2022).
81. Kaiser, H. F. The Varimax criterion for analytic rotation in factor-analysis. *Psychometrika* **23**, 187–200 (1958).
82. Parcellation of vertex-wise maps and spin testing. <https://doi.org/10.17605/OSF.IO/X8QP9>. (2025).

## Acknowledgements

This work was supported in part by the National Institutes of Health (R01DC014021 PI Bonilha; R01DC022458 PI Bonilha; NIHRF1-MH133701 PI Rorden); the statewide Alzheimer’s Disease Research Center Designation funded by the South Carolina Department of Health and Human Services (University of South Carolina Lead; Bonilha); the Aging Brain Cohort Excellence Initiative (PI Fridriksson).

## Author contributions

N.R.: Conceptualization, Methodology, Validation, Formal Analysis, Writing – Original Draft, Visualization. A.T.: Methodology, Software, Resources, Data Curation, Visualization. S.N.N.: Investigation, Resources, Data Curation, Supervision, Project administration. R.N.: Methodology, Investigation,

Resources, Data Curation, Project administration. I.R.: Conceptualization, Data Curation, Writing – Original Draft. C.R.: Software, Resources, Data Curation, Supervision, Project administration, Funding acquisition. J.F.: Conceptualization, Resources, Supervision, Project administration, Funding acquisition. L.B.: Conceptualization, Resources, Supervision, Project administration, Funding acquisition. All authors contributed to writing, review, and editing, and they have approved the manuscript.

## Competing interests

The authors declare no competing interests.

## Additional information

**Supplementary information** The online version contains supplementary material available at <https://doi.org/10.1038/s42003-025-08228-z>.

**Correspondence** and requests for materials should be addressed to Nicholas Riccardi.

**Peer review information** *Communications Biology* thanks Guoyuan Yang and the other anonymous reviewer(s) for their contribution to the peer review of this work. Primary Handling Editors: Jessica Peters and Joao Valente. A peer review file is available.

**Reprints and permissions information** is available at <http://www.nature.com/reprints>

**Publisher’s note** Springer Nature remains neutral with regard to jurisdictional claims in published maps and institutional affiliations.

**Open Access** This article is licensed under a Creative Commons Attribution-NonCommercial-NoDerivatives 4.0 International License, which permits any non-commercial use, sharing, distribution and reproduction in any medium or format, as long as you give appropriate credit to the original author(s) and the source, provide a link to the Creative Commons licence, and indicate if you modified the licensed material. You do not have permission under this licence to share adapted material derived from this article or parts of it. The images or other third party material in this article are included in the article’s Creative Commons licence, unless indicated otherwise in a credit line to the material. If material is not included in the article’s Creative Commons licence and your intended use is not permitted by statutory regulation or exceeds the permitted use, you will need to obtain permission directly from the copyright holder. To view a copy of this licence, visit <http://creativecommons.org/licenses/by-nc-nd/4.0/>.

© The Author(s) 2025